Two-dimensional electron systems and interfacial coupling in $LaCrO_3/KTaO_3$ heterostructures

Athby H. Al-Tawhid[1], Divine P. Kumah[2], and Kaveh Ahadi[1*]

[1]Department of Materials Science and Engineering, North Carolina State University, Raleigh, NC 27695, USA

[2]Department of Physics, North Carolina State University, Raleigh, North Carolina 27695, USA

[*] Corresponding author. Email: kahadi@ncsu.edu

ABSTRACT

The strong interfacial coupling at the 3*d*-5*d* transition metal-oxide interfaces has generated excitement due to the possibility of engineering a wide range of quantum phenomena and functionalities. Here, we investigate the electronic interfacial coupling and structural properties of $LaCrO_3/KTaO_3$ heterostructures. High quality $LaCrO_3$ films were grown on $KTaO_3$ substrates using molecular beam epitaxy. These heterostructures show a robust two-dimensional electron gas and a metallic behavior down to liquid helium temperature. Using magnetoresistance measurements, we analyze the coupling of electronic orders between Cr 3*d* and Ta 5*d* states and observe signatures of weak anti-localization and Kondo scattering at low temperature transport. The results provide direct evidence that a crossover (weak anti-localization to Kondo) occurs with increasing temperature as the dephasing scattering events reduce the coherence length. Our observations allow for a clear and detailed picture of two distinct quantum corrections to conductivity at low temperature.

The discovery of a mobile two-dimensional electron system[1] and its novel functionalities and emergent phenomena[2–7] at the interface of complex oxides motivated efforts to engineer these interfaces as a platform for new physics[8–12]. Recently, the 3*d*-5*d* transition-metal-oxide interfaces have shown promise due to the possibility of the emergence of highly tunable quantum phenomena[13,14]. For example, a tunable topological Hall effect is reported where the strong spin-orbit coupling meets magnetism at these interfaces[15–20]. The experimental realization of the 3*d*-5*d* interfaces, however, has been limited to a few material systems and a strong interfacial coupling remains elusive.

$KTaO_3$ is an incipient ferroelectric[21] with superconductivity emerging at low temperatures in doped samples[22] similar to $SrTiO_3$[23–26]. A combination of a large dielectric constant and small effective mass of electrons, i.e. large effective Bohr radius, could induce a metallic state in $KTaO_3$ even in the dilute doping regimes. A robust two-dimensional electron system has been reported at the interfaces of $KTaO_3$ with $LaTiO_3$[27], $LaVO_3$[28], EuO[29], and $LaAlO_3$[30]. Recently, a nematic two-dimensional superconductivity was discovered at the (111)[31] and (110)[32] $KTaO_3$ interfaces with EuO and $LaAlO_3$. Ta 5*d* driven conduction electrons in $KTaO_3$ have smaller effective mass (~0.3) and higher mobility and spin-orbit coupling compared to Ti 3*d* driven conduction electrons in $SrTiO_3$ [33]. Furthermore, $KTaO_3$ is more susceptible to interfacial coupling, due to the extended Ta 5*d* orbitals, compared to Ti 3*d*. Previously, a polar discontinuity driven two dimensional electron system was observed at the $LaCrO_3/SrTiO_3$ interfaces[34–36]. A polar discontinuity along (001) exists at the $LaCrO_3/KTaO_3$ interface. The $KTaO_3$, has charged planes along (001) direction with alternating $(KO)^{-1}$ and the $(TaO_2)^{+1}$ planes while the $LaCrO_3$ has alternating $(LaO)^{+1}$ and $(CrO_2)^{-1}$ planes along (001). The TaO_2-terminated $LaCrO_3/KTaO_3$ interfaces, as a result, have a polar discontinuity with the same sign but twice the magnitude compared to $LaCrO_3/SrTiO_3$ heterostructures[37]. The $(LaO)^{+1}$ and $(TaO_2)^{+1}$ planes at the interface each donate half electron per interfacial unit cell. These electrons reside in Ta 5*d* driven conduction band of $KTaO_3$ at the interface.

Here, we study the formation of two-dimensional electron systems and probe quantum corrections to conductivity at the $LaCrO_3/KTaO_3$ interface. A combination of polar discontinuity and oxygen vacancy formation creates a two-dimensional electron gas at the $LaCrO_3/KTaO_3$ interfaces. We observe a strong interfacial coupling between Cr 3*d* and Ta 5*d* states. Weak anti-localization and Kondo scattering events dominate the low temperature transport and we observe a crossover between the two regimes at low temperature.

High quality $LaCrO_3$ films were grown on (001) oriented $KTaO_3$ substrates using molecular beam epitaxy (MBE). Prior to growth, the $KTaO_3$ substrates were treated with buffered hydrofluoric acid and annealed in air at 700 ^{o}C in a tube furnace for four hours to create a TaO_2-terminated surface[38]. Atomic force microscope (AFM) images of the substrate before and after treatment show that an atomic-scale terrace step

structure is formed (Supplementary Information). The $LaCrO_3$ films were grown at 1×10^{-7} Torr oxygen partial pressure with the base pressure of the MBE chamber being 2×10^{-10} Torr. The flux of the La and Cr sources were calibrated before the growth using a quartz crystal microbalance. Reflection high energy electron diffraction (RHEED) was used to monitor the growth process. Here, a two-step growth method was used to grow $LaCrO_3$ thin films. First, four unit cells of amorphous $LaCrO_3$ were grown at 600 ^oC (thermocouple temperature). The initial low temperature growth is required to protect the $KTaO_3$ surface from degradation at higher temperatures (>800 ^oC) due to potassium loss as evidenced by RHEED (Supplementary Information)[28]. The initial low temperature growth could also stabilize the polar/polar interface in $LaCrO_3/KTaO_3$ heterostructures. The substrate is then heated to 900 ^oC at which point the $LaCrO_3$ crystallizes. The remaining $LaCrO_3$ is deposited at 900 ^oC. Figure 1(a) and (b) show the RHEED images of the initial $KTaO_3$ surface and after the growth of 20 u.c. of $LaCrO_3$. The streaky diffraction pattern of $LaCrO_3$ in Figure 1(b) indicates a two-dimensional growth. The in-plane pseudo-cubic lattice constant of bulk $LaCrO_3$, 3.87 Å [39], matches the $KTaO_3$ lattice constant, 3.99 Å [40]. The growth, as a result, shows a pseudo-cube on cube structure and, if fully strained, the $LaCrO_3$ displays a 3% in-plane compressive strain.

To confirm the film crystallinity and determine the film lattice constants, X-ray diffraction (XRD) $\theta - 2\theta$ scans of the $LaCrO_3$(40u.c.s)/$KTaO_3$ were performed using a Rigaku SmartLab X-ray diffractometer. Figure 1(c) shows the wide-angle scans performed (15^o-55^o) along the 00L direction, confirming that the heterostructure is epitaxial, (001)-oriented, and single phase. A zoom-in near the 001- and 002-diffraction peaks shows the well-defined peaks of $LaCrO_3$ and $KTaO_3$, confirming the high structural crystallinity and quality of the $LaCrO_3$ films. The $LaCrO_3$ out of plane lattice constant is 3.83 Å which is smaller than the bulk value of 3.88 Å [39] due to the biaxial in-plane tensile stress.

Electrical transport measurements were performed using a square Van der Pauw configuration in the range of 3-300 K. Gold contacts were deposited using a sputter system at the corners of the samples through a shadow mask. All transport measurements were performed using a Quantum Design physical property measurement system (PPMS). The temperature dependence of the sheet resistance (R_{xx}) for $LaCrO_3$(20u.c.s)/$KTaO_3$ immediately after the growth shows a metallic behavior, $\frac{dR}{dT} > 0$, down to 3 K (Supplementary Information). The Hall measurements at 300 K and 10 K for the $LaCrO_3$(20u.c.s)/$KTaO_3$ sample from which the sheet carrier concentration, n_s, and mobility, μ, are determined. It shows a weak temperature dependence of the sheet carrier density with n_s=1.15×14 cm^{-2} at 300 K and 7.3×13 cm^{-2} at 10 K, revealing a robust 2D electron gas in these heterostructures. The temperature dependence may suggest a weak carrier trapping. It also could be a result of the particular behavior of transverse and longitudinal scattering rates in the complex oxide films, as discussed elsewhere[20,41,42]. The carrier mobility increase from

17 cm^2/Vs at room temperature to 140 cm^2/Vs at 10 K. Here, the Hall carrier density could be due to a combination of the polar discontinuity and oxygen vacancies induced during growth. The sample was exposed to air for one week to fill the oxygen vacancies before carrying out remaining experiments. Figure 2 (a) and (b) show the temperature dependence of the sheet resistance and carrier density, respectively. The sheet carrier density decreases (~33%) with atmospheric exposure, due to filling of oxygen vacancies in $KTaO_3$. Sample did not show any change in carrier density after one week onward. Furthermore, oxygen annealing (250 ^oC for two hours) did not show any change in carrier density, confirming that oxygen vacancy formation during growth and polar discontinuity contribute to the formation of electron system in as-grown sample. The theory predicted carrier density from polar catastrophe, i.e. one electron per interfacial unit cell, overestimates the Hall carrier density. Similar behavior has been observed in $LaTiO_3/KTaO_3$[27], $LaCrO_3/SrTiO_3$[34], and $LaAlO_3/SrTiO_3$[7]. The discrepancy could be attributed to the presence of charged defects. The sheet resistance/carrier mobility increases/decreases with atmospheric exposure and a resistance upturn emerges around 15 K. The relatively fast filling of the oxygen vacancies, i.e. Hall carrier density loss, at room temperature is attributed to higher oxygen vacancy formation energy in $KTaO_3$, compared to $SrTiO_3$[43]. A capping layer is required to protect the oxygen vacancies induced during growth[31].

Figure 3 shows the longitudinal magnetoresistance of the $LaCrO_3$(20u.c.s)/$KTaO_3$ at different temperatures (3 K, 15 K, 60 K). A positive magnetoresistance emerges at 3 K similar to previous reports of two-dimensional electron systems on $KTaO_3$ [30,44]. We attribute this positive magnetoresistance to weak anti-localization (WAL). The WAL occurs when the coherence length becomes larger than the elastic mean free path ($l_\varphi \gg l_{el}$) and, as a result, the self-crossing paths of charge carriers could interfere[45–47]. The Berry curvature in momentum space generates a π phase shift for closed trajectories, resulting in WAL. The phase shift occurs due to (pseudo)spin-momentum locking. A negative parabolic magnetoresistance emerges at higher temperature. The negative magnetoresistance is a signature of Kondo scattering[48]. The Cr 3*d* spins scatter the Ta 5*d* conduction electrons at the interface. The resistance upturn observed at ~15 K is another signature of Kondo scattering. A Kondo fit to the resistance upturn shows a very good agreement with the theory of Kondo scattering [49,50]. The Kondo upturn is only obvious after the oxygen vacancies that are far from the interface are filled. The $TiO_x/KTaO_3$ heterostructures were also grown using MBE. The two-dimensional electron gas at these interfaces do not show signatures of Kondo scattering and a transition from WAL to classical magnetoresistance response is observed with increasing temperature (Supplementary Information).The competition between WAL and Kondo scattering dominates the longitudinal magnetoresistance at low temperatures. The conductivity change with temperature and magnetic field is given by:

$$\Delta\sigma_{xx}^{T}(B,T) = ne\mu\left[\frac{1}{(1+\mu^2B^2)}-1\right] + \Delta\sigma_{xx}^{WAL} + \Delta\sigma_{xx}^{Kondo},$$

where the longitudinal conductivity is obtained from $\sigma_{xx} = \rho_{xx}/\left[\rho_{xx}^2 + \rho_{xy}^2\right]$. The first term represents the classical magnetoresistance response, ignoring the spin-orbit and Zeeman contributions, followed by WAL and Kondo responses, respectively.

Next, we discuss the effect of Rashba spin-orbit coupling on the Kondo scattering at the $LaCrO_3/KTaO_3$ interfaces. In the presence of spin-orbit coupling, the Cr 3*d* exhibits static spin correlations with the nonzero orbital angular momentum conduction electrons at the interface. The electron system derived from Ta 5*d* has roughly one order of magnitude larger spin-orbit interaction compared to Ti 3*d*. A resistance upturn also emerges at the $LaCrO_3/SrTiO_3$ interfaces at similar temperature range after oxygen anneal[34]. It is predicted that the Kondo temperature increases exponentially with Rashba spin-orbit coupling[51]. Here, the Kondo temperature shows a weak dependence to Rashba spin-orbit coupling.

In summary, our experimental results, especially the temperature dependence of the longitudinal magnetoresistance, should be of interest for testing the different theoretical models that have been proposed and guiding future experiments for coupling of the electronic orders across the 3*d*/5*d* transition metal oxide interfaces[13,18,52–54]. We have shown high quality $LaCrO_3/KTaO_3$ heterostructures grown using a two-step MBE growth method. A two-dimensional electron system is formed due to a combination of polar discontinuity, at the $LaCrO_3/KTaO_3$ (100) interface, and oxygen vacancy formation (n_s~1×14 cm^{-2}). The proximity to Cr 3*d* introduces Kondo scattering events. The competition between WAL and Kondo scattering dominates the electronic transport at liquid helium temperature. Finally, it would be interesting to explore the interplay between the high spin-orbit coupling of $KTaO_3$ and the proximitized magnetic fluctuations at the $LaCrO_3/(111)KTaO_3$ superconducting interfaces.

See the supplementary material for the AFM and RHEED data, and the magnetoresistance of the $TiO_x/KTaO_3$ two-dimensional electron systems.

Transport measurements were supported by NC-State University startup funds. Film growth was supported by the U.S. National Science Foundation under Grant No. NSF DMR-1751455.

Data availability statement

The data that support the findings of this study are available from the corresponding author upon reasonable request.

Reference:

[1] A. Ohtomo and H.Y. Hwang, Nature **427**, 423 (2004).

[2] N. Reyren, S. Thiel, A.D. Caviglia, L.F. Kourkoutis, G. Hammerl, C. Richter, C.W. Schneider, T. Kopp, A.-S. Rüetschi, D. Jaccard, M. Gabay, D.A. Muller, J.-M. Triscone, and J. Mannhart, Science **317**, 1196 (2007).

[3] A.D. Caviglia, S. Gariglio, C. Cancellieri, B. Sacépé, A. Fête, N. Reyren, M. Gabay, A.F. Morpurgo, and J.-M. Triscone, Phys. Rev. Lett. **105**, 236802 (2010).

[4] K. Ahadi and S. Stemmer, Phys. Rev. Lett. **118**, 236803 (2017).

[5] H. Chandrasekar, K. Ahadi, T. Razzak, S. Stemmer, and S. Rajan, ACS Appl. Electron. Mater. acsaelm.9b00738 (2020).

[6] K. Ahadi, O.F. Shoron, P.B. Marshall, E. Mikheev, and S. Stemmer, Appl. Phys. Lett. **110**, (2017).

[7] A.D. Caviglia, S. Gariglio, N. Reyren, D. Jaccard, T. Schneider, M. Gabay, S. Thiel, G. Hammerl, J. Mannhart, and J.-M. Triscone, Nature **456**, 624 (2008).

[8] R. Mori, P.B. Marshall, K. Ahadi, J.D. Denlinger, S. Stemmer, and A. Lanzara, Nat. Commun. **10**, (2019).

[9] P. Moetakef, J.R. Williams, D.G. Ouellette, A.P. Kajdos, D. Goldhaber-Gordon, S.J. Allen, and S. Stemmer, Phys. Rev. X **2**, 021014 (2012).

[10] J. Chen, G. Wang, Y. Tang, J. Xu, X. Dai, J. Jia, W. Ho, and M. Xie, (2016).

[11] A.D. Caviglia, M. Gabay, S. Gariglio, N. Reyren, C. Cancellieri, and J.-M. Triscone, Phys. Rev. Lett. **104**, 126803 (2010).

[12] K. Ahadi, H. Kim, and S. Stemmer, APL Mater. **6**, (2018).

[13] K. Huang, L. Wu, M. Wang, N. Swain, M. Motapothula, Y. Luo, K. Han, M. Chen, C. Ye, A.J. Yang, H. Xu, D.C. Qi, A.T. N'Diaye, C. Panagopoulos, D. Primetzhofer, L. Shen, P. Sengupta, J. Ma, Z. Feng, C.W. Nan, and X. Renshaw Wang, Appl. Phys. Rev. **7**, 011401 (2020).

[14] S. Okamoto, J. Nichols, C. Sohn, S.Y. Kim, T.W. Noh, and H.N. Lee, Nano Lett. **17**, 2126 (2017).

[15] N. Mohanta, E. Dagotto, and S. Okamoto, Phys. Rev. B **100**, 064429 (2019).

[16] Y. Li, L. Zhang, Q. Zhang, C. Li, T. Yang, Y. Deng, L. Gu, and D. Wu, ACS Appl. Mater. Interfaces **11**, 21268 (2019).

[17] S. Bhowal and S. Satpathy, Phys. Rev. B **99**, 245145 (2019).

[18] E. Skoropata, J. Nichols, J.M. Ok, R. V. Chopdeka, E.S. Choi, A. Rastogi, C. Sohn, X. Gao, S. Yoon, T. Farmer, R.D. TDesautel, Y. Choi, D. Haskel, J.W. Freelan, S. Okamoto, M. Brahlek, and H.N. Lee, Sci. Adv. **6**, eaaz3902 (2020).

[19] J. Nichols, X. Gao, S. Lee, T.L. Meyer, J.W. Freeland, V. Lauter, D. Yi, J. Liu, D. Haskel, J.R. Petrie, E.J. Guo, A. Herklotz, D. Lee, T.Z. Ward, G. Eres, M.R. Fitzsimmons, and H.N. Lee, Nat. Commun. **7**, 1 (2016).

[20] K. Ahadi, X. Lu, S. Salmani-Rezaie, P.B. Marshall, J.M. Rondinelli, and S. Stemmer, Phys. Rev. B **99**, (2019).

[21] A.R. Akbarzadeh, L. Bellaiche, K. Leung, J. Íñiguez, and D. Vanderbilt, Phys. Rev. B - Condens. Matter Mater. Phys. **70**, 054103 (2004).

[22] K. Ueno, S. Nakamura, H. Shimotani, H.T. Yuan, N. Kimura, T. Nojima, H. Aoki, Y. Iwasa, and M. Kawasaki, Nat. Nanotechnol. **6**, 408 (2011).

[23] S. Salmani-Rezaie, K. Ahadi, W.M. Strickland, and S. Stemmer, Phys. Rev. Lett. **125**, 087601 (2020).

[24] S. Salmani-Rezaie, K. Ahadi, and S. Stemmer, Nano Lett. **20**, 6542 (2020).

[25] K. Ahadi, L. Galletti, Y. Li, S. Salmani-Rezaie, W. Wu, and S. Stemmer, Sci. Adv. **5**, eaaw0120 (2019).

[26] R. Russell, N. Ratcliff, K. Ahadi, L. Dong, S. Stemmer, and J.W. Harter, Phys. Rev. Mater. **3**, (2019).

[27] K. Zou, S. Ismail-Beigi, K. Kisslinger, X. Shen, D. Su, F.J. Walker, and C.H. Ahn, APL Mater. **3**, 036104 (2015).

[28] S. Goyal, N. Wadehra, and S. Chakraverty, Adv. Mater. Interfaces **7**, 2000646 (2020).

[29] H. Zhang, Y. Yun, X. Zhang, H. Zhang, Y. Ma, X. Yan, F. Wang, G. Li, R. Li, T. Khan, Y. Chen, W. Liu, F. Hu, B. Liu, B. Shen, W. Han, and J. Sun, Phys. Rev. Lett. **121**, 116803 (2018).

[30] H. Zhang, H. Zhang, X. Yan, X. Zhang, Q. Zhang, J. Zhang, F. Han, L. Gu, B. Liu, Y. Chen, B. Shen, and J. Sun, ACS Appl. Mater. Interfaces **9**, 36456 (2017).

[31] C. Liu, X. Yan, D. Jin, Y. Ma, H.-W. Hsiao, Y. Lin, T.M. Bretz-Sullivan, X. Zhou, J. Pearson, B. Fisher, J.S. Jiang, W. Han, J.-M. Zuo, J. Wen, D.D. Fong, J. Sun, H. Zhou, and A. Bhattacharya, Science (80-.). eaba5511 (2021).

[32] Z. Chen, Z. Liu, Y. Sun, X. Chen, Y. Liu, H. Zhang, H. Li, M. Zhang, S. Hong, T. Ren, C. Zhang, H. Tian, Y. Zhou, J. Sun, and Y. Xie, Phys. Rev. Lett. **126**, 026802 (2021).

[33] V.R. Cooper, Phys. Rev. B - Condens. Matter Mater. Phys. **85**, 235109 (2012).

[34] A. Al-Tawhid, J.R. Frick, D.B. Dougherty, and D.P. Kumah, J. Vac. Sci. Technol. A **37**, 021102 (2019).

[35] A.H. Al-Tawhid and D.P. Kumah, AIP Adv. **10**, 045132 (2020).

[36] Y.P. Hong, X.X. Wang, G.L. Qu, C.J. Li, H.X. Xue, K.J. Liu, Y.C. Li, C.M. Xiong, R.F. Dou, L. He, and J.C. Nie, Chinese Phys. B **27**, 047301 (2018).

[37] J. Thompson, J. Hwang, J. Nichols, J.G. Connell, S. Stemmer, and S.S.A. Seo, Appl. Phys. Lett. **105**, 102901 (2014).

[38] H.J. Bae, J. Sigman, D.P. Norton, and L.A. Boatner, Appl. Surf. Sci. **241**, 271 (2005).

[39] H.E. Höfer and Wulf F. Kock, J. Electrochem. Soc. **140**, 2889 (1993).

[40] H. Uwe, H. Unoki, Y. Fujii, and T. Sakudo, Solid State Commun. **13**, 737 (1973).

[41] P.B. Marshall, K. Ahadi, H. Kim, and S. Stemmer, Phys. Rev. B **97**, 155160 (2018).

[42] K. Ahadi, L. Galletti, and S. Stemmer, Appl. Phys. Lett. **111**, (2017).

[43] J. Xi, H. Xu, Y. Zhang, and W.J. Weber, Phys. Chem. Chem. Phys. **19**, 6264 (2017).

[44] N. Wadehra, R. Tomar, R.M. Varma, R.K. Gopal, Y. Singh, S. Dattagupta, and S. Chakraverty, Nat. Commun. **11**, 1 (2020).

[45] M. Dzero, M.G. Vavilov, K. Kechedzhi, and V.M. Galitski, Phys. Rev. B - Condens. Matter Mater. Phys. **92**, 165415 (2015).

[46] H.-Z. Lu and S.-Q. Shen, Spintron. VII **9167**, 91672E (2014).

[47] A. Al-Tawhid, A.-A. Shafe, P. Bagheri, Y. Guan, P. Reddy, S. Mita, B. Moody, R. Collazo, Z. Sitar, and K. Ahadi, Appl. Phys. Lett. **118**, 082101 (2021).

[48] Y. Katayama and S. Tanaka, Phys. Rev. **153**, 873 (1967).

[49] J.R. Schrieffer and P.A. Wolff, Phys. Rev. **149**, 491 (1966).

[50] J. Kondo, Prog. Theor. Phys. **32**, 37 (1964).

[51] M. Zarea, S.E. Ulloa, and N. Sandler, Phys. Rev. Lett. **108**, 046601 (2012).

[52] T.S. Suraj, G.J. Omar, H. Jani, M.M. Juvaid, S. Hooda, A. Chaudhuri, A. Rusydi, K. Sethupathi, T. Venkatesan, A. Ariando, and M.S.R. Rao, Phys. Rev. B **102**, 125145 (2020).

[53] T. Yu, Q. Liu, P. Chen, L. Zhou, H. Li, X. Ning, C. Qiu, and H. He, J. Alloys Compd. **789**, 351 (2019).

[54] S. Bhowal and S. Satpathy, in *AIP Conf. Proc.* (American Institute of Physics Inc., 2018), p. 020007.

Figure Captions

Figure 1. Structural Characterization of $LaCrO_3/KTaO_3$ heterostructure. (a) and (b) are RHEED of the $KTaO_3$ substrate prior to growth and $LaCrO_3$(40u.c.s)/$KTaO_3$ after the growth, respectively. (c) XRD $\theta - 2\theta$ scan along the 001 peak of the $LaCrO_3$(40u.c.s)/$KTaO_3$ heterostructure.

Figure 2. Electronic transport of $LaCrO_3/KTaO_3$ heterostructure. (a) and (b) sheet resistance and Hall results of the $LaCrO_3$ (20u.c.s)/$KTaO_3$ heterostructure after growth. (c) and (d) sheet resistance and sheet carrier density of the $LaCrO_3$(20u.c.s)/$KTaO_3$ heterostructure with temperature after exposure to atmosphere. Inset: emergence of an upturn at 12 K.

Figure 3. Magnetoresistance of $LaCrO_3/KTaO_3$. Longitudinal magnetoresistance of $LaCrO_3$(20u.c.s)/$KTaO_3$ with out-of-plane magnetic field at 3 K, 15 K, and 60 K.

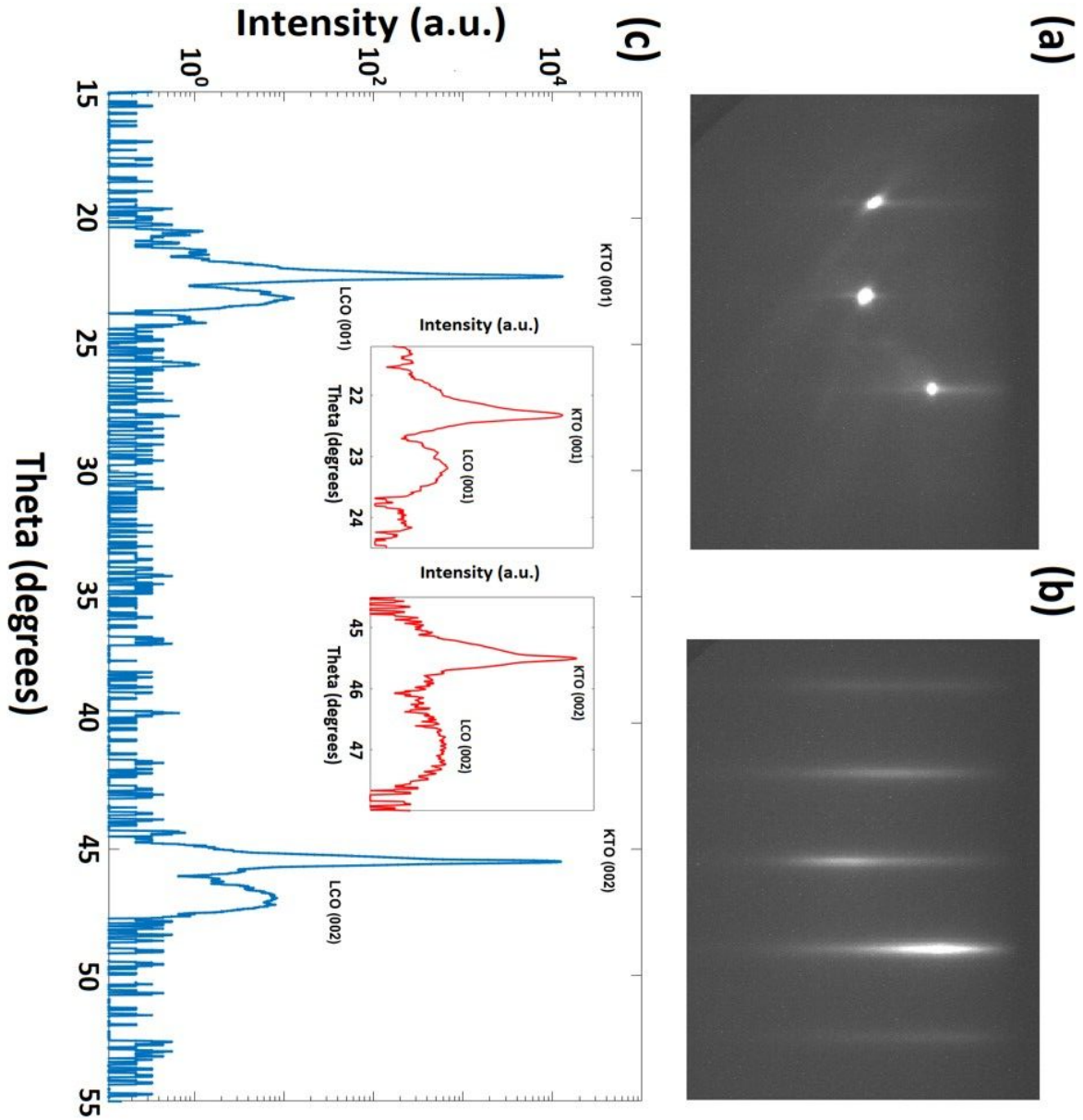

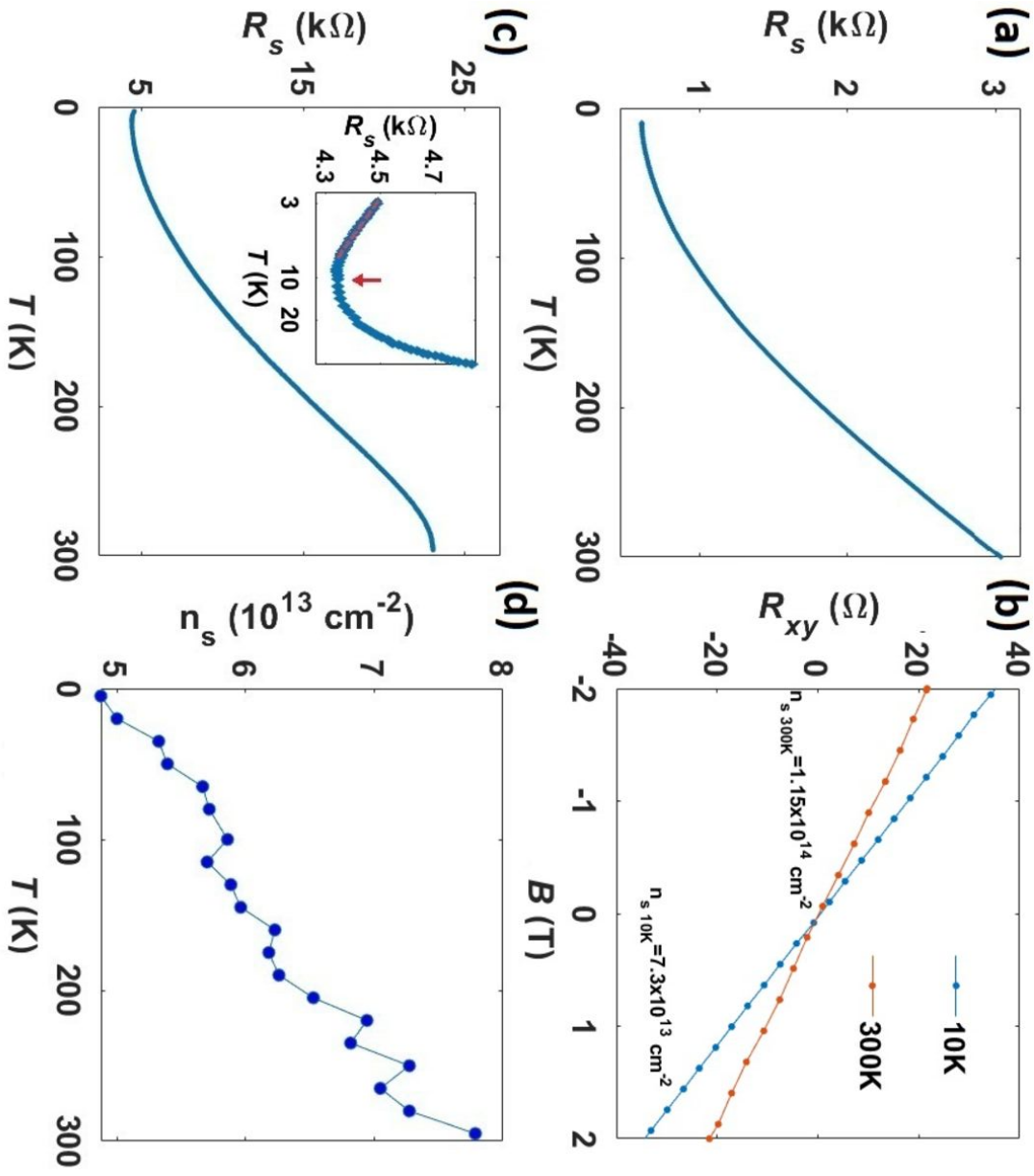

PLEASE CITE THIS ARTICLE AS DOI: 10.1063/5.0049119